The June–September Low Cloud Cover in Western Central Africa: Mean Spatial Distribution and Diurnal Evolution, and Associated Atmospheric Dynamics

A. DOMMO

Laboratory of Environmental Modeling and Atmospheric Physics, University of Yaoundé 1, Yaoundé, Cameroon

N. PHILIPPON

IGE, University of Grenoble Alpes, CNRS, IRD, Grenoble INP, Grenoble, France

DERBETINI A. VONDOU

Laboratory of Environmental Modeling and Atmospheric Physics, University of Yaoundé 1, Yaoundé, Cameroon

G. SÈZE

LMD, IPSL, UPMC, CNRS, EP, ENS, Paris, France

R. EASTMAN

Department of Atmospheric Sciences, University of Washington, Seattle, Washington

(Manuscript received 15 February 2017, in final form 23 March 2018)

ABSTRACT

Western central Africa (WCA) was recently shown to be one of the cloudiest areas of the tropics. Analyzing an ensemble of satellite products and surface cloud observations, we show that in June–September, WCA cloud cover is dominated by single-layered low stratiform clouds. Despite an underestimation of low cloud frequency in satellite estimates at night, comparisons with surface observations bring insights into the spatial distribution and diurnal cycle of low clouds. Both appear strongly influenced by orography: to the west, the coastal plains and the ocean-facing valleys have the largest cloud cover and a lower-amplitude diurnal cycle with a maximum cloud phase at 0400 local time (LT). To the east, across the windward slopes, plateaus, and downwind slopes, the cloud cover becomes progressively reduced and the diurnal cycle has a larger amplitude with a maximum cloud phase at 1000 LT. In terms of atmospheric dynamics, the east/west gradient observed in low cloud frequency and amount is related to a foehn effect without substantial rainfall on windward slopes. The diurnal cycle of low clouds on the windward slopes and plateaus is related to the reversal, from mean subsidence at 0700 LT over the Atlantic and inland to rising motion inland at 1300 LT. In addition, the airmass stability in low levels prevents the vertical development of cloud cover. Last, we could not detect in the European reanalyses any nocturnal jet as observed in southern West Africa (SWA), suggesting different mechanisms triggering low cloud formation in WCA compare to SWA.

1. Introduction

Clouds are important components of weather and climate. Clouds modulate water and energy budgets through rainfall and solar/terrestrial radiation. However, clouds are one of the most challenging aspects for climate modeling (Bony et al. 2015). Simulated cloud fields still present large biases as compared to satellite observations, and models show wide intermodel spread

Denotes content that is immediately available upon publication as open access.

Supplemental information related to this paper is available at the Journals Online website: https://doi.org/10.1175/JCLI-D-17-0082.s1.

Corresponding author: A. Dommo, dmmatanas@gmail.com

DOI: 10.1175/JCLI-D-17-0082.1

(Jiang et al. 2012; Lauer and Hamilton 2013). The unrealistic representation of cloud cover is the main source of uncertainty in global warming projections (Dufresne and Bony 2008). This is particularly so for low stratiform clouds, which are among the least well-simulated clouds by climate models. Low stratiform clouds play a critical role in energy budgets, as they emit longwave radiation at a similar temperature to the land surface, but they also scatter visible solar radiation. Their importance combined with their poor representation in models induces large biases in simulated energy budgets [see Cheng and Xu (2015), and references within].

In the tropics low stratiform clouds are common over the eastern basins of the subtropical oceans (Klein and Hartmann 1993; Eastman and Warren 2014), where sea surface temperatures are cold and the thermal inversion that caps the planetary boundary layer (PBL) is strong. They are also frequently observed over the neighboring arid coastal areas, for example, in California (Pilié et al. 1979; Torregrosa et al. 2016), Chile (Muñoz et al. 2016), and Namibia (Cermak 2012), where they are particularly important from an ecosystem perspective. Indeed, by lowering the temperatures and bringing a substantial amount of water (in the form of fog mainly) to these arid coastal areas, clouds sustain forests where they otherwise would not be observed (García-Santos et al. 2004; Del-Val et al. 2006). The annual cycle of low clouds is closely tied to the annual cycle of static stability, while their diurnal cycle usually shows a peak near sunrise and moderate amplitude (Eastman and Warren 2014).

Apart from these abovementioned areas (eastern basins of the subtropical oceans and their coastal margins), low stratiform clouds are not the dominant cloud type in the tropics. This especially holds true over tropical land areas (Eastman and Warren 2014). Therefore, most of studies dedicated to cloud cover over tropical land—and Africa in particular—focus on the high opaque clouds (e.g., cumulonimbus) and the related mesoscale convective systems (MCSs; e.g., Jackson et al. 2009; Kamsu-Tamo et al. 2014; Laing et al. 2008; Sassen et al. 2009; Vondou et al. 2010). Indeed, these systems and associated clouds bring much of the yearly rainfall to the tropics, so year-to-year variations in amount are critical for ecosystem viability and societies. However, in tropical Africa a region has been shown to stand apart from this general pattern: southern West Africa (SWA), that is, the region extending from Ivory Coast to Nigeria and up to 9°N. During July–September (JAS), SWA is regularly covered by low stratiform clouds (Knippertz et al. 2011; Schrage and Fink 2012; van der Linden et al. 2015). The latter studies, based on a combination of satellite estimations and in situ observations, point to a specific spatial evolution of this cloud cover along the diurnal cycle. It is at its minimum at 1800 LT, with the largest frequencies of occurrence [20%–30% according to Meteosat Second Generation (MSG) retrievals] confined to the coast (south of 6°–7°N). After sunset the cover thickens and extends northward through 10°N until the next day at around 1000 LT (with frequencies of occurrence reaching ~40%). After 1000 LT the cover thins out, opens (or even breaks up into fair-weather cumuli along its northern edge), and dissipates in the afternoon. This diurnal evolution is different from that of the maritime stratus over the Gulf of Guinea: there, the stratiform clouds dissipate more rapidly in the early morning. The formation of a nocturnal low-level jet (NLLJ) is a key factor for the nighttime development of low clouds in SWA (Schrage et al. 2007; Schrage and Fink 2012; Schuster et al. 2013): the associated wind shear enhances mechanically the vertical mixing of the air mass. The impact of cloud cover on the water budget is significant. Low stratiform clouds are usually nonprecipitating, contributing to the relative dryness of the JAS season in SWA (locally referred to as "the little dry season"). They also substantially impact the incoming solar and outgoing terrestrial radiation (e.g., SWA receives only 150 W m^{-2} in JAS; i.e., half as much radiation as the Sahel region farther north), and therefore surface temperature (Knippertz et al. 2011; Schuster et al. 2013). A correct simulation of this cloud cover by climate models is therefore of importance. However, Hannak et al. (2017) analyzing simulations from an ensemble of models participating in CMIP5 noted large biases and a large spread between models in the simulation of the cover of low clouds as compared to ERA-Interim. The simulated cloud cover is too high and displays a too-weak diurnal cycle. Most of the models also overestimate the NLLJ, and the associated dry and cold advection.

In this study we show that the neighboring region of western central Africa (WCA; Fig. 1) is also frequently blanketed by low stratiform clouds from June to September.

WCA is the region extending from ~6°S–5°N, 8°–18°E, bounded to the south by the Congo River, to the north by the Cameroonian volcanic rift, to the west by the Atlantic, and to the east by the Congo and Ubangi Rivers. It encompasses part of Cameroon, the Central African Republic (CAR), the Democratic Republic of the Congo (DRC), the Republic of Congo, Equatorial Guinea, and Gabon. The topography is dominated by plateaus (e.g., Batéké) and massifs (e.g., Chaillu, Crystal) of medium altitude (~500–900 m MSL) incised by rivers such as Sanaga and Ogooué. These plateaus are relatively close to the coast, particularly in Cameroon

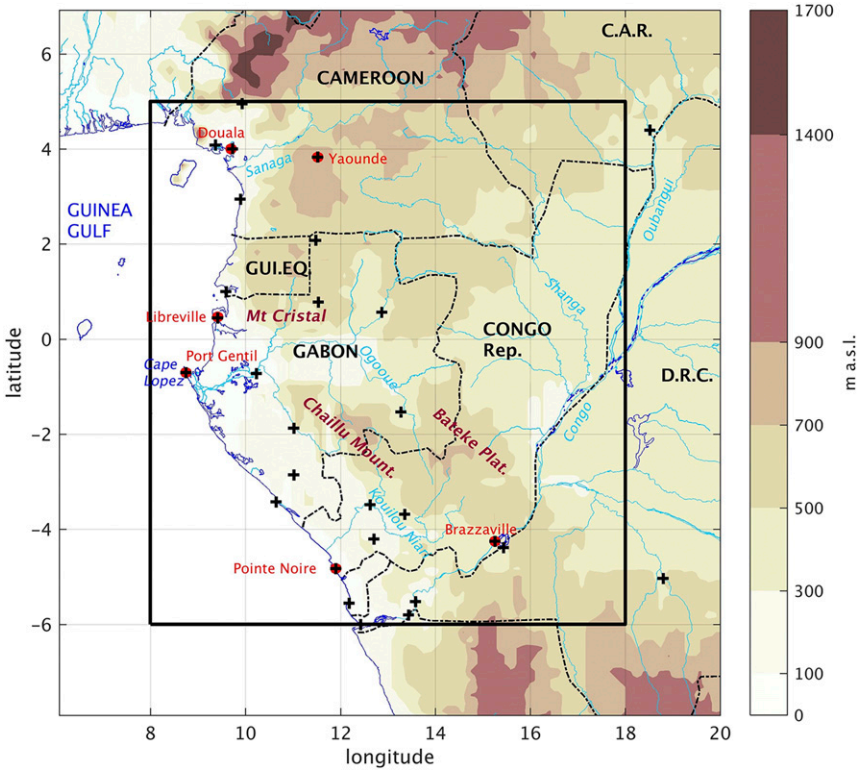

FIG. 1. Main geographical aspects of WCA and topography (levels displayed: 100, 300, 500, 700, 900, 1400, and 1700 m; brown shadings). EECRA stations selected for analysis (black crosses) and the study domain (black box) are marked.

and Equatorial Guinea, so the coastal plain is narrow, while in Gabon the coastal plain is larger, ~100 km. This marks an important contrast compared to SWA, where low-lying flatlands extend farther inland. WCA is also mainly covered by dense evergreen forests (Mayaux et al. 2013), which keep a substantial amount of moisture in the PBL; this marks a second important contrast with SWA, which is covered by more degraded and open deciduous forests.

WCA is one of the cloudiest regions of the tropics as recently described by Wilson and Jetz (2016) using ~1-km-resolution monthly cloud frequencies from Moderate Resolution Imaging Spectroradiometer (MODIS) retrievals: The mean annual cloud frequency is around 80%, a value also obtained by Philippon et al. (2016) for north Republic of Congo using cloud data from MSG. Moreover and interestingly, in the study by Eastman and Warren (2014), WCA also stands out as one of the regions of the world where the amplitude of the diurnal cycle of low clouds is very large. Low clouds in the humid tropics have long been recognized by botanists and foresters as important for forest traits and functioning. In particular, low clouds sustain so-called tropical cloud forests (Oliveira et al. 2014). However, even though there are 97 sites listed in central Africa (https://www.unep-wcmc.org/resources-and-data/tropical-montane-cloud-forest-sites), no in-depth study has been done on the low cloud cover in WCA to date.

Therefore, the objective of this study is to improve understanding of the large low-topped cloud cover that develops between June and September in WCA. In particular, the questions we seek to answer are, How frequent are these clouds over the region in June–September (JJAS) and what is their spatial distribution? How do they evolve along the diurnal cycle? What are the atmospheric conditions that explain their presence and evolution throughout the diurnal cycle? To that end we analyze an ensemble of satellite, surface-based, and reanalysis products, which are briefly described in section 2. Section 3 presents the results. The mean spatial patterns of low clouds in JJAS and their mean evolution during the diurnal cycle are presented in section 3a. The potential biases in the cloud products used are analyzed in section 3b. Section 3c depicts the associated atmospheric dynamics and sea surface temperatures. Last, in section 4, conclusions are drawn.

2. Data

a. Cloudiness data

To document the low cloud cover in WCA, three products are analyzed. Two are issued from satellite retrievals; that is, clouds are seen from the top and their type is determined from their top temperature or pressure. One is from surface observations; that is, clouds are seen from the land surface, and their type (morphology) is determined by trained observers. The three products are 1) the cloud type (CT) product processed by the Satellite Application Facility for Supporting Nowcasting and very short range forecasting (SAFNWC) from MSG retrievals, 2) the global climate model–oriented *Cloud–Aerosol Lidar and Infrared Pathfinder Satellite Observations* (*CALIPSO*) cloud product issued from the Cloud–Aerosol Lidar with Orthogonal Polarization (CALIOP) retrievals, and 3) the Extended Edited Synoptic Cloud Reports Archive (EECRA).

1) THE SAFNWC CT PRODUCT

The SAFNWC CT product is issued from the SAFNWC/MSG algorithms (see http://www.nwcsaf.org/web/guest/scientific-documentation) using Spinning Enhanced Visible and Infrared Imager (SEVIRI) bidirectional reflectances (R) and brightness temperatures (BT) for 10 channels (high-resolution visible plus three channels in visible—R0.6 μm, R0.8 μm, R1.6 μm; and six channels in infrared—BT3.9 μm, BT7.3 μm, BT8.7 μm, BT10.8 μm, BT12.0 μm, BT13.4 μm), combined with sun and satellite angles, numerical weather prediction (NWP) model forecast and climatological fields of sea surface temperatures, surface temperature, air temperature at five levels (950, 850, 700, 500 hPa, plus at the tropopause level), total water vapor content of the atmosphere, and the altitude of the NWP grid, and land/sea/coast/altitude atlases (Derrien and Le Gléau 2005, 2010).

This product offers a classification of clouds into 14 classes, at 3-km spatial resolution and 15-min resolution over the Europe–Africa disk. The classes are organized from the altitude of the cloud top, and for high clouds, on an indication of their semitransparency (Table 1). For our study purposes, the focus is put on the low-topped clouds, but the mid- and high-topped clouds are also considered for interpretation. Note that the pixels classified as fractional clouds have been reallocated to the cloud class when the majority of the eight neighboring pixels is covered with such clouds. As low clouds are frequent over WCA and fractional clouds are usually portions of high semitransparent clouds—thin cirrus—or low broken clouds, the percentage of low clouds after reallocation is significantly increased from ~12 to ~18% (Table 1).

TABLE 1. The main classes of clouds in the SAFNWC CT product. Low-topped clouds, which are of interest, are in bold. Medium- and high-topped clouds, which are also considered for interpretation, are in italics. The percentage of clouds before and after reallocation of partial clouds is given in the second and third columns, respectively [see text in section 2a(1)].

TYPE OF CLOUD	Before	After
Cloud-free land pixels not contaminated by snow or ice	29.4	29.4
Very low and low clouds	**12.4**	**18.3**
Medium clouds	*3.3*	*3.3*
High and very opaque clouds	*8.9*	*8.9*
Thin semitransparent clouds	*38.1*	*40.2*
Medium thick semitransparent clouds		
Thick semitransparent clouds		
Semitransparent clouds above low or medium clouds		
Fractional clouds (i.e., portion of thin cirrus or low broken clouds)	7.9	0
Others (undefined pixels and nonprocessed data)	0.1	0.1

The cloud type algorithm is a threshold algorithm applied at the pixel scale. It is based on the use of a cloud mask and spectral and textural features computed from the multispectral satellite images and compared with a set of thresholds. The set of thresholds to be applied depends mainly on the illumination conditions, whereas the values of the thresholds themselves may depend on the illumination, the viewing geometry, the geographical location, and NWP data describing the water vapor content and a coarse vertical structure of the atmosphere. First, clear pixels are separated from cloudy pixels. Then opaque clouds are separated from semitransparent clouds and fractional clouds using brightness temperature differences (BT10.8 μm − BT12.0 μm, BT8.7 μm − BT10.8 μm, or BT3.9 μm − BT10.8 μm) and reflectance R0.6 μm (at daytime). Opaque clouds are then separated into very low-level, low-level, midlevel, high-level, or very high-level clouds using 10.8-μm brightness temperatures that are compared to NWP forecast air temperatures at various pressure levels (see Product User Manual for "Cloud Products," http://www.nwcsaf.org/AemetWebContents/ScientificDocumentation/Documentation/MSG/SAF-NWC-CDOP2-MFL-SCI-PUM-01_v3.2.3.pdf).

For our study purposes, the SAFNWC CT product is theoretically the best suited because it samples the diurnal cycle at a high resolution (every 15 min) and also offers a high spatial resolution of 3 km. However, the very low and low clouds, referred to as "low clouds" or "ultra-low and low clouds" (ULLC), are the most challenging ones to detect from passive sensors. It may be difficult to properly detect them in WCA in the following cases: 1) a low solar elevation at twilight (the tests that use the difference between the 10.8- and

3.9-μm channels, which are the most efficient ones to detect low clouds at night, become inoperative in the presence of solar radiation), 2) if low clouds are covered by very thin cirrus (they may be classified as medium cloud), 3) in nighttime conditions when land surface temperature is similar to the cloud-top temperature of the overlying low clouds (note also that surface temperatures as obtained from reanalyses or forecasts are more uncertain in WCA than in other regions because of a few in situ measurements to assimilate). The high water vapor content in the atmospheric lower layers may also play on the expected difference between the clouds and land surface brightness temperatures. Low clouds may also be classified as medium clouds in the presence of a strong thermal inversion. In this later case, to reduce the likelihood of misclassifying low clouds as medium clouds, medium clouds are not allowed to present too large of a difference between BT7.3 μm and BT10.8 μm, which are particularly sensitive to the vertical increase of water content in the low atmosphere. Last, the atmosphere above WCA is also regularly charged with aerosols in January–February and June–September (aerosols optical depth > 2; Torres et al. 2002), issued from biomass burnings during the dry seasons in the neighboring open-forest regions (Roberts et al. 2009). There are at least two ways by which aerosols can bias low clouds detection in SAFNWC: 1) through an impact on the surface temperature—if that impact is not well taken into account into the reanalyses and forecasts used in the SAFNWC detection algorithm, then low clouds will not be properly detected; and 2) through an impact on the clear-sky reflectance. The value taken as reference to separate clear scenes from cloudy scenes can be too high or too low depending on the aerosol loading. Second, a large aerosol load can also smooth spatial disparities in visible irradiance and bias the detection toward a clear sky instead of low small fractioned clouds.

For this study CT data are extracted for the region bounded by latitudes 6°S–5°N and longitudes 6.125°–18°E, for the period 2009–14. Each pixel is assigned a cloud type, meaning that 1) the cloud amount in the pixel is considered to be 100% and 2) at the pixel scale, only the frequency of occurrence of a cloud type can be computed, for example, the fraction of times in a month a cloud is detected or the fraction of days a cloud is detected over a given set of days (this also holds true for the CALIOP cloud product described below). The product is referred to as ''SAFNWC.''

2) CALIOP CLOUD TYPE PRODUCT

The GCM-Oriented *CALIPSO* Cloud Product (GOCCP) is one of the two gridded cloud climatologies derived from CALIOP retrievals (http://climserv.ipsl.polytechnique.fr/cfmip-obs/goccp_v3.html). The lidar CALIOP is on board the sun-synchronous polar-orbiting *CALIPSO* platform that is flying in the A-train constellation. The overpass times of the heliosynchrone orbit of the A-train constellation are 0130 LT and 1330 LT. CALIOP is a near-nadir-viewing, two-wavelength (532 and 1064 nm), polarization-sensitive lidar designed to provide high-resolution (30 m) vertical profiles each 333 m along the *CALIPSO* track of aerosols and clouds in the troposphere and lower stratosphere at global scale (Winker et al. 2009). From the backscatter profiles, the vertical distribution of the cloud cover can be retrieved until the level where the backscatter signal is fully attenuated. The lidar detects very thin upper-layer clouds as soon as their optical thickness is above 0.01 for the daytime observations and 0.002 for the nighttime observations (McGill et al. 2007), and the backscatter signal is fully attenuated when the optical thickness of the cloud profile observed above reaches a value between 3 and 5. The low-level clouds are detectable as soon as they are not covered by a spatially and optically dense upper-layer cloud.

GOCCP (Chepfer et al. 2013; Guzman et al. 2017) was built from an algorithm designed for the goal of evaluating the representation of clouds in climate models, and it employs the following five steps: (i) compute the 532-nm molecular return signal that would be measured in a cloud-free and aerosol-free atmosphere (''ATBmol''); (ii) average the *CALIPSO* level 1 attenuated backscatter lidar profiles (''ATB'') to 40 vertical levels every 480 m, retaining the full horizontal along-track resolution (1/3 km); (iii) compute the scattering ratio profile; (iv) for each profile detect the presence of clouds at each 480-m level (the pixel is declared cloudy when attenuated scattering ratio (SR) > 5 and ATB-ATBmol $> 2.5 \times 10$–$3\,\mathrm{km^{-1}\,sr^{-1}}$); and (v) accumulate the cloudy and clear pixels within each grid box (typically 2° latitude × 2° longitude, Chepfer et al. 2013). For our study purposes we used the global maps of high, middle, and low cloud fractions obtained with GOCCP, version 2, at 2° × 2° spatial resolution for the period 2007–15, and extracted the WCA region. To determine the frequency of opaque midlevel and high-level clouds under which low-level clouds are not detectable, we used the z_opaque_fraction parameter included in GOCCP, version 3.0 (Guzman et al. 2017). The GOCCP–CALIOP products are referred to as ''CALIOP.'' Note that low clouds in CALIOP are not single-layered ''low-topped cloud'' only as in SAFNWC. Instead, they are single-layered-plus-multilayered low clouds, as they can be detected below optically thin high clouds thanks to the CALIOP sensor.

3) EECRA

The EECRA offers a cloud climatology for land during the period 1971–2009. The EECRA is processed from reports taken by trained observers on all continents at 5388 land-based synoptic weather stations for both day and night. In this database the cloud type is determined by the observer based on the base height and the physical characteristics of the cloud. The documentation explaining the processing of the synoptic reports and the various products and files available can be found online (at www.atmos.washington.edu/CloudMap).

WCA is documented by 28 EECRA stations, shown as black crosses in Fig. 1. For our study purposes we used four cloud products: The multiyear monthly averages of cloud frequency (MMCF) and cloud amount (MMCA), and the multiyear seasonal averages of cloud frequency (MSFT) and cloud amount (MSAT) for eight observation times per day. The four products provide the frequency or amount of cloud for the total cloud cover and for nine different types of clouds at three levels. These types and levels are as follows: high-level clouds; mid-level clouds: nimbostratus, altostratus, and altocumulus; and low-level clouds: fog, stratus, stratocumulus, cumulus, and cumulonimbus. In the EECRA, cumulonimbus are classified as low clouds because their base height is of the same order as that of other low clouds, though we acknowledge that their vertical extent is often greater than other low clouds. Cloud amount in the EECRA indicates sky-dome cover of a given type of cloud. Cloud frequency indicates the fraction of observations when a given type is observed.

The MMCF and MMCA provide monthly averages of cloud frequency and amount, respectively, for nighttime only, daytime only, and the day–night average. We selected the months of June–September. The total low-level clouds and the stratus are studied. The MSFT and MSAT provide cloud frequency and amount, respectively, for eight synoptic hours (0000–2100 UTC in steps of 3 h, that is, 0100–2200 LT for WCA) averaged over the seasons December–February (DJF), March–May (MAM), June–August (JJA), and September–October (SON). We selected the JJA season and the low-level clouds for analysis (note that the JJAS period is not available in the MSFT/MSAT format). The number of reports available for computing MMCF/MMCA and MSFT/MSAT varies among the stations and throughout the diurnal cycle. Stations of the DRC and the 2200, 0100, and 0400 LT synoptic hours are less frequently observed (Figs. S1 and S2 in the online supplemental material). Note also that there is only a one-year overlap between the period documented by the EECRA and that documented by SAFNWC. However, we assume that the climatologies obtained from the two products are built from a sufficient number of observations to give reasonable and comparable estimates.

b. Atmospheric dynamics and sea surface temperatures

1) ERA-STF

As a near-observational modeling reference, short-term forecasts made in the production of the European Centre for Medium-Range Weather Forecasts (ECMWF) interim reanalysis (ERA-STF; Dee et al. 2011) have been used. The advantages of using ERA-STF are (i) a 3-hourly time resolution (started at 0000 UTC every day) and (ii) a physically consistent diurnal cycle using the model forecast times. Data are provided by ECMWF at a 25-km spatial resolution (after a linear interpolation from the ERA-Interim 75-km original resolution). We extracted the zonal, meridional, and vertical components of the wind, relative humidity, temperature, and the low cloud fraction for the region 6°S–5°N, 8°–18°E and for the period 2009–14. Cloud type in ERA-STF is determined using a set of thresholds applied to sigma, the ratio of pressure to surface pressure. Clouds are considered low when $1 > \text{sigma} > 0.8$. The low cloud cover in the ERA-STF may be occasionally biased (underestimated mainly) in the presence of multiple cloud layers (see https://www.ecmwf.int/en/faq/how-are-low-medium-and-high-cloud-cover-defined; there are a number of issues with the cloud fraction profile and the low cloud fraction diagnostics).

To highlight zonal overturning circulations that develop over the region in JJAS, and following Cook and Vizy (2016), we computed the divergent component of the zonal wind and multiplied it by the vertical pressure velocity. At the seasonal scale, ERA wind fields were shown to be consistent with those from NCEP-2 and MERRA reanalyzes for central Africa (Pokam et al. 2014). Despite the limited in situ atmospheric dynamics data available for the region, Nicholson and Grist (2003) show that the 700-mb reanalyzed climatological winds from NCEP-2 are in good agreement with observations.

2) OSTIA SST

Sea surface temperatures (SST) are obtained from the Operational Sea Surface Temperature and Sea Ice Analysis (OSTIA; Donlon et al. 2012). OSTIA provides high-spatial-resolution (5 km) daily SST data for the global ocean, obtained by combining satellite [Advanced Very High Resolution Radiometer (AVHRR)] and in situ SST [International Comprehensive Ocean–Atmosphere Data Set (ICOADS)] measurements. Data are extracted for the eastern southern tropical Atlantic

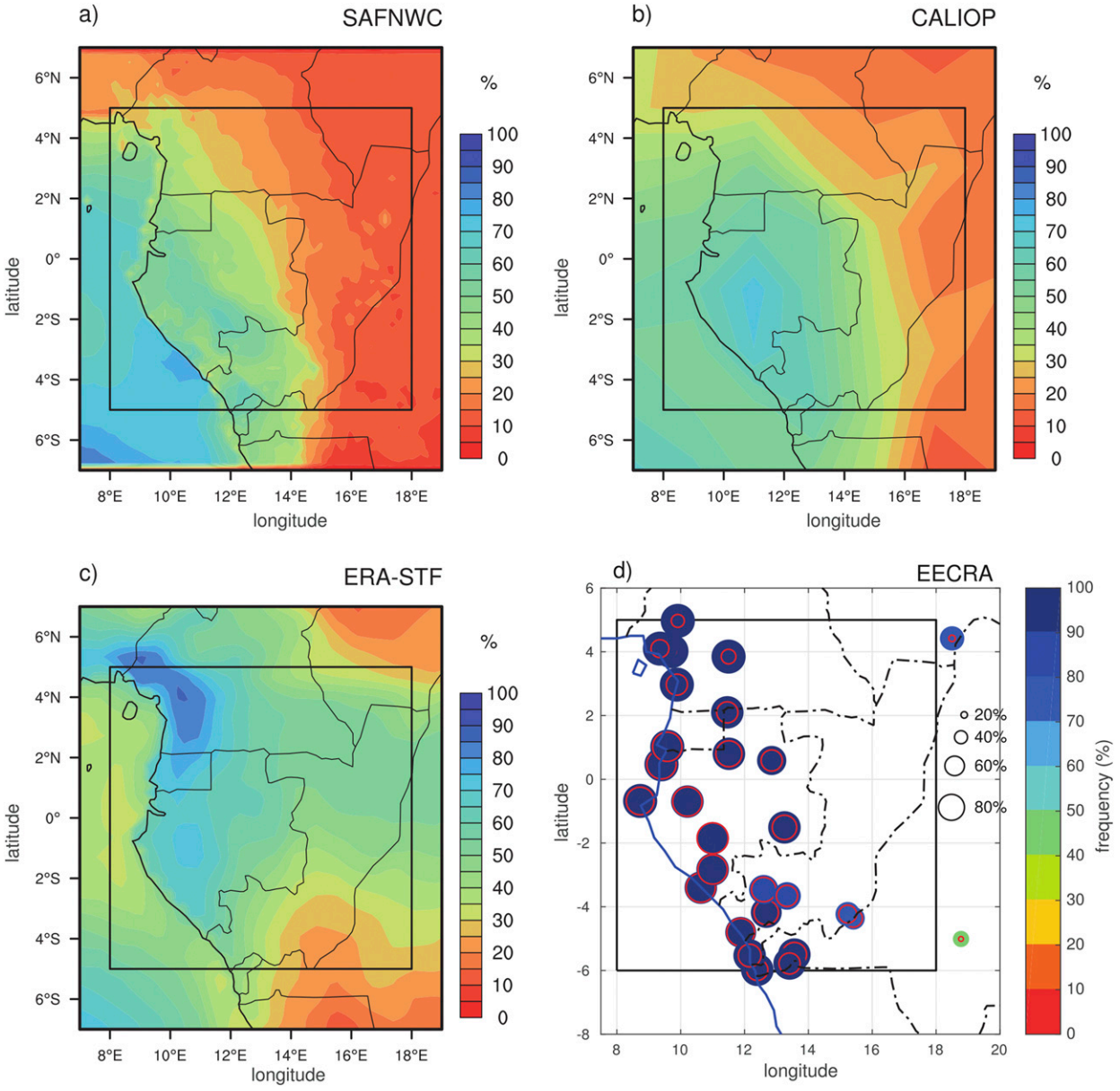

FIG. 2. ULLC frequency (%) in JJAS and for nighttime and daytime, from (a) SAFNWC (2009–14), (b) CALIOP (2007–15), (c) ERA-STF (2009–14), and (d) EECRA (1971–2009). In (d), the circle size is proportional to the frequency. The total low clouds (blue disks) and the low stratiform clouds only (red circles) are marked.

only (8°N–30°S, 0°–6°E) over the period 2009–14 and are upscaled to the monthly time step.

3. Results

a. Low cloud JJAS mean spatial patterns and diurnal evolution

1) JJAS MEAN SPATIAL PATTERN

Figure 2 displays the mean frequency of total low clouds in JJAS over WCA as obtained from SAFNWC (Fig. 2a), CALIOP (Fig. 2b), ERA-STF (Fig. 2c), and EECRA (Fig. 2d) compiled using both nighttime and daytime observations (see Fig. S3 in the supplementary materials for nighttime- and daytime-only patterns in SAFNWC, CALIOP, and ERA-STF). Two points are remarkable from Figs. 2a–d: total low cloud frequencies are very high in WCA in JJAS and their spatial pattern partly matches with the topography. SAFNWC shows the lowest cloud frequencies with a maximum value around 50% compared with maxima of 70% shown by both CALIOP and ERA-STF. The EECRA gives the

largest frequencies, with stations in Gabon reporting low cloud frequencies above 80%. The spatial distribution of the highest frequencies is concordant between SAFNWC and CALIOP: clouds appear most frequently on the westward-facing flanks of the Crystal and Chaillu Mountains (Fig. 1). However, in the EECRA the largest frequencies are recorded over the coastal plains and in ERA-STF over the Douala coastal region in Cameroon. Complicating the comparison, the cloud cover over the coastal plains is featured only during daytime by ERA-STF and SAFNWC (Fig. S3). The rapid decrease of ULLC frequency from west to east around 15°E corresponds to the downward slopes facing east toward the Congo basin. The dissipation of ULLC there may allude to different atmospheric processes at play, in particular a weaker influence of the Atlantic and a larger influence of the Congo basin, where the atmospheric conditions sustain MCSs (Jackson et al. 2009). However, in ERA-STF, this decrease around 15°E is not properly reproduced: ULLC frequencies stay around 40%. ULLC frequency decreases more gradually toward Cameroon. EECRA data suggest that the type of low cloud changes from stratiform to more cumuliform clouds (cf. the blue disks size with the red ones in Fig. 2d). This sector is under the influence of other phenomena, such as the West African monsoon (WAM) and the orographic ascent along the Cameroon volcanic ridge, both of which favor the development of high-o00paque-topped clouds.

2) MEAN DIURNAL CYCLE

To best describe and display the mean diurnal cycle of low clouds in SAFNWC, and to highlight the spatial differences in their amplitude and phase, a *k*-means clustering is applied to the mean diurnal cycles for land-only pixels (see the supplementary materials for the methodology). When applying the *k*-means routine, we consider daytime values only, because they are less uncertain than the nighttime ones [cf. section 3b(2)]. The results are presented in Fig. 3 with a clustering into four types of diurnal cycles (ranging from 0100 to 2400 LT). Figure 3a presents their distribution in WCA, Fig. 3b their shape, and Fig. 3c the range of altitudes at which they are observed. These four types are distributed mainly from west to east (Fig. 3b) following the main geographical features: coast and low-lying ocean-facing valleys, windward flanks, plateaus, and Congo basin margins. The main differences between the four types (Fig. 3b) relate to the frequencies of cloudiness, with a gradual decrease seen toward the east. Pixels located to the west in coastal plains and ocean-facing valleys (~200 m MSL; Fig. 3c) display frequencies of low clouds as high as 70% at 1300 LT compared to 25% for pixels located on the western margin of the Congo basin (~400 m MSL). Pixels located on the windward flanks of plateaus (~500 m MSL) and plateaus (~600 m MSL) display frequencies lower than those in coastal plains (40% and 58% vs 70%) but also different phases: the peak is reached earlier, ~1000 LT (vs 1300 LT).

To compare low cloud diurnal cycles obtained from SAFNWC with those seen by EECRA, we extracted the SAFNWC pixels documenting EECRA stations using 3×3 pixels around stations (i.e., ~9 km $\times$ 9 km). Then we grouped them according to their belonging to one of the four regions displayed in Fig. 3a and computed the respective mean diurnal cycle for the low cloud amount. The amounts are calculated by averaging the binary (cloudy vs noncloudy) pixel data for all nine pixels. We also grouped the EECRA stations according to their belonging to one of the four regions (note however that there is not any EECRA station documenting the Congo basin margins—compare Fig. 1—so that region is omitted) and computed the respective mean diurnal cycles for low cloud amounts. Diurnal cycles obtained for these two datasets are presented in Fig. 4. Note first that diurnal cycles computed from the collocated SAFNWC pixels (Fig. 3a) and those documenting EECRA stations only (Fig. 4a) are not similar in terms of amplitude for the coast and plateaus, and the phases show some modest differences as well. At night, the amounts of cloudiness do not compare well between the EECRA and SAFNWC pixels. This holds particularly true for the stations/pixels located in coastal plains. Whereas EECRA gives cloudiness amounts $> 70\%$ and a flat cycle (amplitude $< 10\%$, Fig. 4b), the amounts and amplitude in SAFNWC (Fig. 4a) are much lower ($<45\%$, the difference with EECRA always $>30\%$; Fig. 4c) and much larger (20%). The agreement between the two sources is somewhat better for the phases of the cycles although there is a systematic shift toward 1100 LT in SAFNWC as compared to 0600 LT in EECRA (see also Figs. S4 and S5, which provide the differences between the eight synoptic hours for EECRA and SAFNWC). Nonetheless, the comparison of regions suggests that diurnal cycles of low clouds are stronger over plateaus and windward slopes than in the coastal plains and valleys.

Although there are fewer nighttime observations available at EECRA stations (Figs. S1 and S2), the results suggest that low cloud cover during nighttime is much larger than what is pictured by SAFNWC. For instance, for pixels/stations located in coastal plains and windward slopes, the difference in the amount of low clouds between SAFNWC and EECRA is as large as ~45% during nighttime (with the largest difference—$>50\%$—around sunrise) versus ~30% during daytime

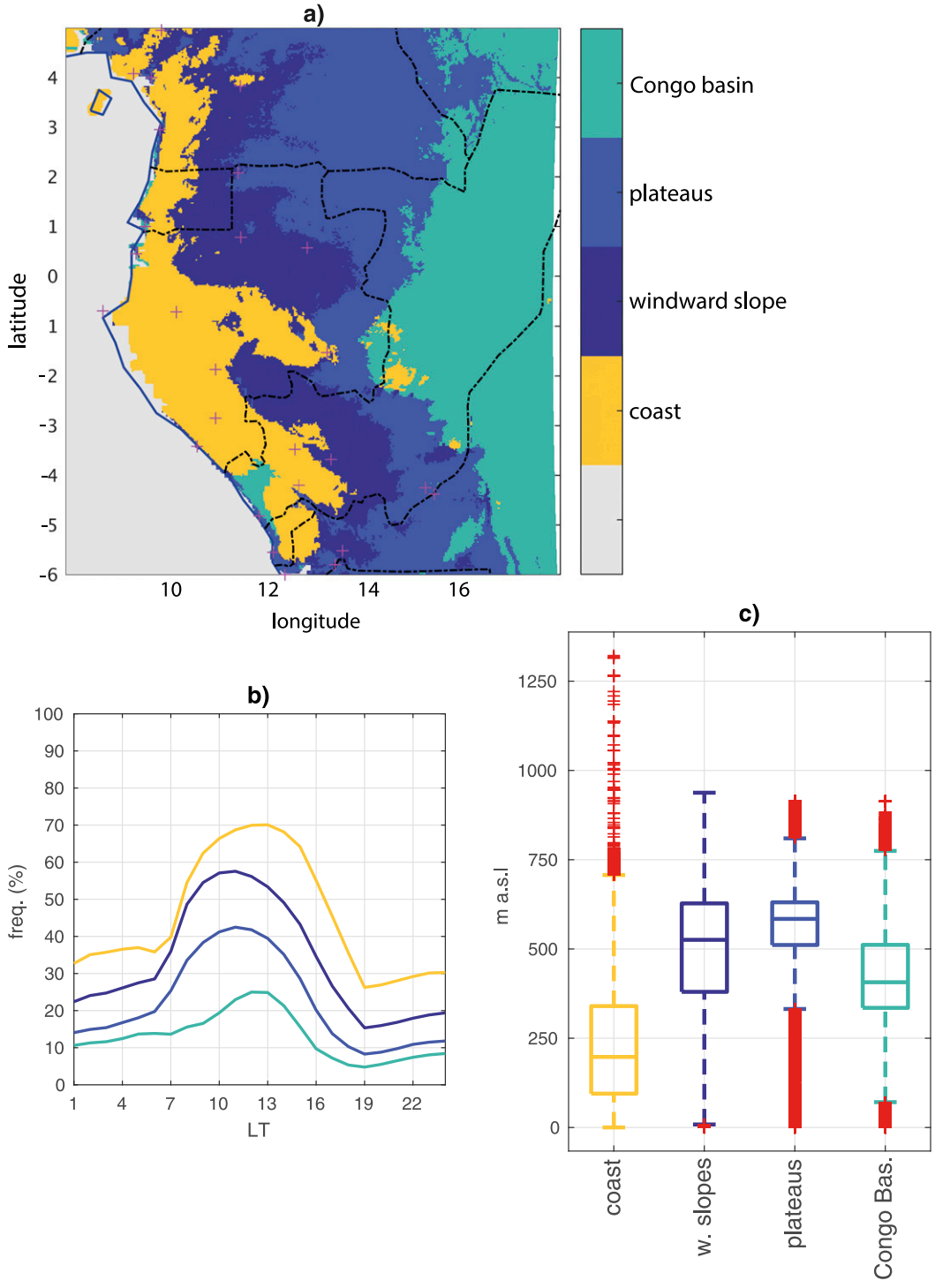

FIG. 3. *K*-means clustering of the ULLC diurnal cycle for land pixels only using SAFNWC (period 2009–2014). (a) Spatial distribution of the four classes (coast, windward slopes, plateaus, Congo basin) plus EECRA stations (magenta crosses). (b) Corresponding diurnal cycle [plus that of ocean pixels (dashed line)]. (c) Boxplots of the altitude of the pixels falling into the four classes [with the 25th and 75th percentiles as the lower and upper limits of the box, respectively; the median (line in the box); and outliers (red crosses)].

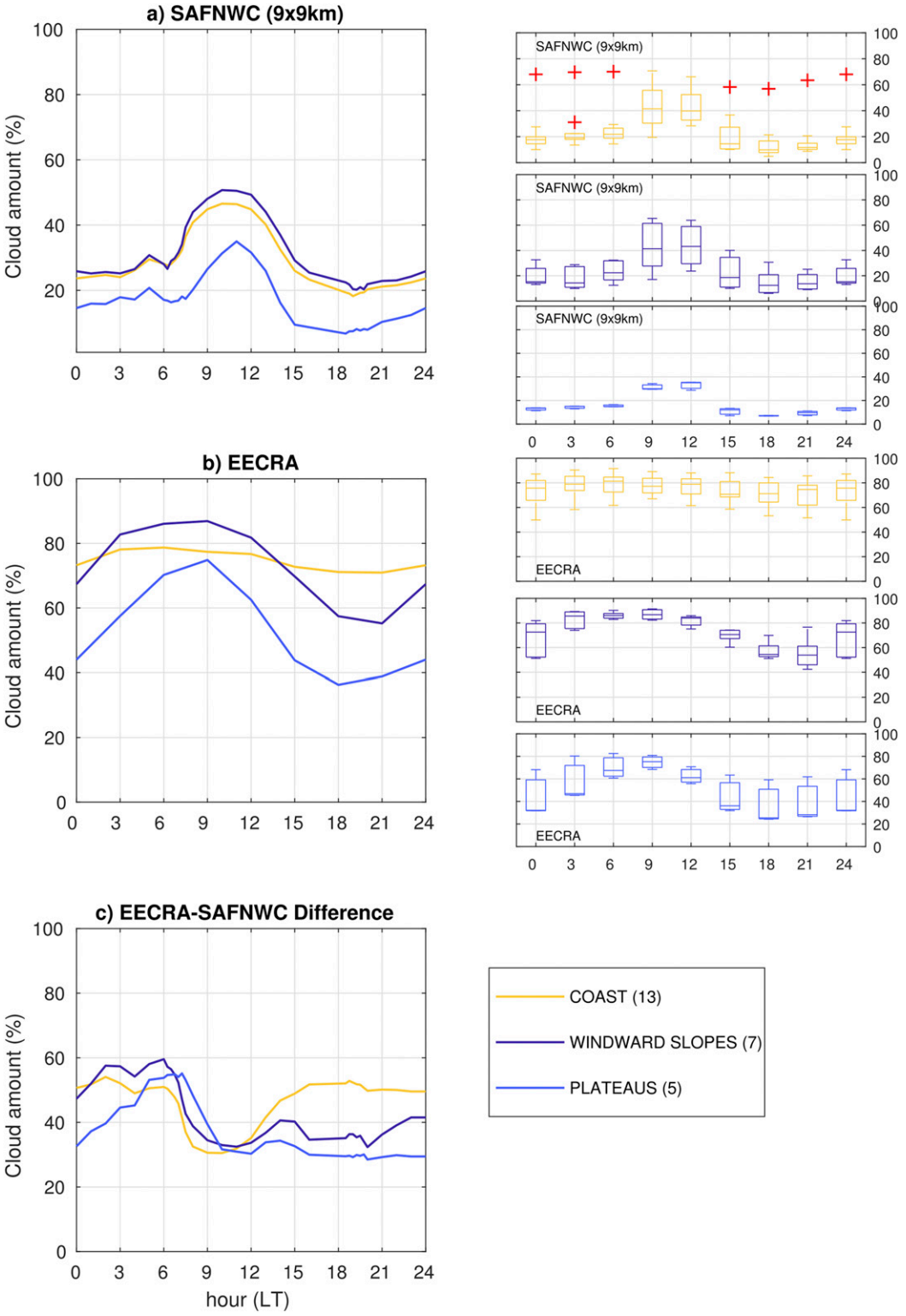

FIG. 4. (left) Diurnal cycles of ULLC amounts in the coastal plains, windward slopes, and plateaus subregions from (a) SAFNWC pixels documenting the EECRA stations (3 × 3 pixels around stations), (b) EECRA stations, and (c) difference between EECRA and SAFNWC. (right) Boxplots of the cloud amount considering all the pixels (for SAFNWC) or stations (for EECRA) for each of the three subregions [with the 25th and 75th percentiles as the lower and upper limits of the box, respectively; the median (line in the box); and outliers (red crosses)].

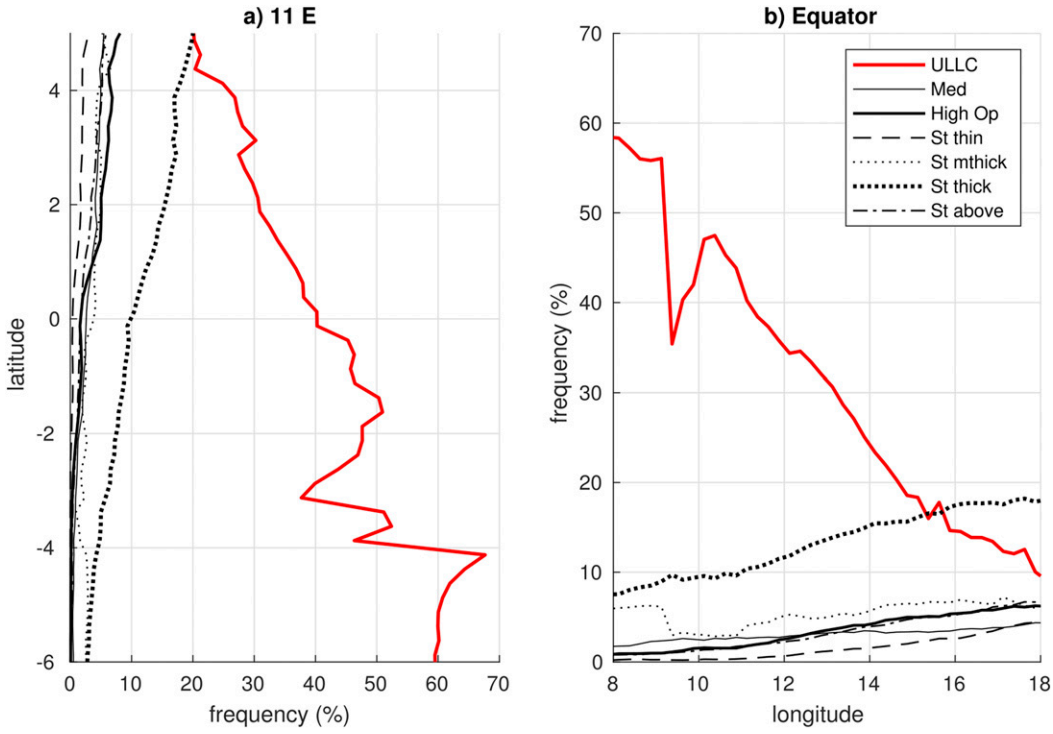

FIG. 5. Frequency in JJAS of ultralow and low (ULLC), medium (Med), high opaque (High Op), and four types of high semitransparent clouds (thin, semithick, thick, above clouds) in SAFNWC (2009–14). (a) Along a meridional transect by 11°E. (b) Along a longitudinal transect by 0°.

(Fig. 4c). Although ERA-STF displays much higher ULLC frequencies at night as compared to SAFNWC (Fig. S3), ULLC in ERA-STF are restricted to the windward slopes and Mount Chaillu, which are mainly where frequencies reach 90% at 0300 LT (vs 45% above the coastal plains).

Beyond differences between EECRA and SAFNWC in ULLC amounts and phase of the diurnal cycles, differences are also observed in the spatial spread of pixels/stations. The right panels in Fig. 4 give for each subregion (coast, windward slopes, and plateaus) and the two products (SAFNWC and EECRA) the spread of cloud amount (as boxplots) between stations for EECRA and pixels for SAFNWC along the diurnal cycle. In EECRA the largest spatial spread is observed at nighttime, especially for windward slopes and plateaus, and could be related to the fewer nighttime observations. In SAFNWC, the largest spatial spread is observed from 0900 to 1500 LT, when ULLC amounts are maximal. It is the weakest for the plateaus, where ULLC amounts are the smallest, and it suggests a more uniform spatial dynamics of clouds there as compared to the coast and windward slopes. To the contrary in EECRA the spatial spread is the largest for the plateaus, but there are only five stations available.

b. *Potential biases in the detection of low clouds in SAFNWC*

The underestimation of low clouds by SAFNWC as compared to the other products may come from the presence of higher clouds masking them, or their nondetection. These two aspects are explored in the following subsections.

1) CLOUDS OVERLAPPING

Two-layered clouds, especially high clouds layered with stratus or stratocumulus, are the most frequent situation of cloud overlapping at low latitudes as shown by Li et al. (2015) and Subrahmanyam and Kumar (2016) using CALIOP retrievals. Therefore, the frequencies of high and medium clouds over WCA are checked.

Figure 5 presents, for the SAFNWC data first, the mean frequencies of ULLC, and medium and high opaque clouds, and four types of high semitransparent clouds over the study region along a meridional (Fig. 5a) and a zonal (Fig. 5b) transect. There is little chance of medium or high opaque clouds masking the low clouds over the region. The frequencies of medium and high opaque clouds in SAFNWC are below 5%, except for

the northernmost (Fig. 5a; 5°N, i.e., foot of the Cameroon volcanic ridge) and easternmost (Fig. 5b; 18°E, i.e., longitude of the Congo basin) sectors. But for these two sectors, for any product considered (SAFNWC, CALIOP, ERA-STF, or EECRA, Fig. 2), the low clouds are less frequent.

To ensure the infrequent occurrence of low- and midlevel cloud layers preventing the observation of low clouds, we show in Fig. 6 the frequencies of medium and high opaque clouds in CALIOP, that is, clouds with an optical thickness > 5 present above 3.2 km and below which the lidar signal is fully attenuated. They compare with the SAFNWC medium clouds, high opaque clouds, and thick semitransparent clouds reported in Fig. 5.

In CALIOP, as in SAFNWC, these medium and high opaque clouds that can mask underlying low clouds are not frequent over WCA (<25% on average) except for the northernmost and easternmost sectors. The frequencies are ~50% and 30%, respectively (vs ~33% and 30%, respectively, for the cumulated frequencies of medium, high opaque, and thick semitransparent clouds in SAFNWC; Fig. 5). These findings suggest that the large underestimation of low cloud amounts in SAFNWC as compared to EECRA (Fig. 4) in the coastal plains of Gabon in particular is mainly due to nondetection when present because of either 1) the influence of aerosols, 2) the thresholds used for nighttime detection, or 3) spatial-scale issues, rather than overlapping by high opaque clouds.

2) NIGHTTIME DETECTION

As discussed in the data section, nighttime detection of low clouds from passive infrared imagers is challenging in WCA, where land surface temperature at night is close to the temperature of the overlying low cloud tops. Figure 4c clearly illustrates this failure, as low clouds amounts computed from SAFNWC at nighttime are largely below what is provided by EECRA (differences of ~45%). In addition, discontinuities around 0600 and 1900 LT (i.e., sunrise and sunset, respectively) in Fig. 4a also point to failures in low cloud detection over WCA at low solar elevation.

The first point suggests that the thresholds used in SAFNWC to detect ULLC during nighttime are not appropriate for WCA. van der Linden et al. (2015) have obtained for SWA better detection of ULLC by lowering the threshold used in the BT10.8 μm − BT3.9 μm test to a constant value of 2 K. Following van der Linden et al. (2015), a new set of thresholds based on brightness temperatures, referred to as "BT," is established for the BT10.8 μm − BT3.9 μm test over WCA and is applied for the years 2012–14 only. To take into account the spatial variations in integrated water vapor content, the thresholds are chosen for each pixel, for each month and hour, according to the distribution of the differences between BT10.8 μm and BT3.9 μm, when ULLC are detected in SAFNWC during this month. For a given pixel p and a given hour h of a given month m, if

$$(\mathrm{BT10.8}\,\mu\mathrm{m})\mathrm{ph} > 283\mathrm{K} \text{ (as in van der Linden et al. 2015) and}$$
$$\mathrm{thresh1} < (\mathrm{BT10.8}\,\mu\mathrm{m} - \mathrm{BT3.9}\,\mu\mathrm{m})\mathrm{ph} < \mathrm{thresh2},$$

then a clear pixel is reclassified as a low cloud. The values of thresh1 and thresh2 are, respectively, the minimum and maximum of the distribution of BT10.8 μm − BT3.9 μm differences.

Using these new thresholds (denoted as BT9km), the amount of low clouds ~9 km around EECRA stations (i.e., 3 × 3 pixels) from ~1900 to ~0600 LT are first compared to the amounts obtained using the standard thresholds (CT9km; Fig. 7, black curves). On average, applying these new thresholds leads only to a moderate increase (~5%) in low cloud detection during nighttime, suggesting that these thresholds are still too conservative. The increase is slightly larger for pixels located on windward slopes and plateaus than for coastal plains. This could be due to larger day-to-day variations in total water vapor content over windward slopes and plateaus than coastal plains.

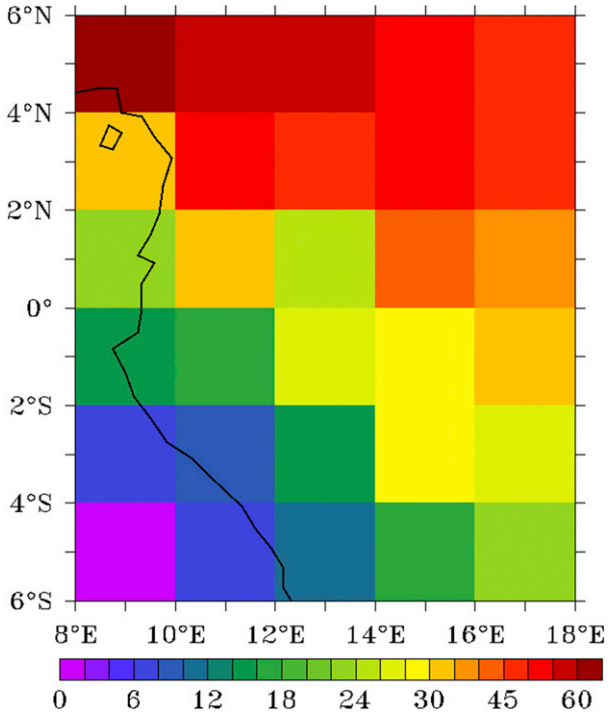

FIG. 6. Frequencies of optically thick (>5) clouds above 3.2 km MSL in JJAS as detected with nighttime CALIOP data (2007–15).

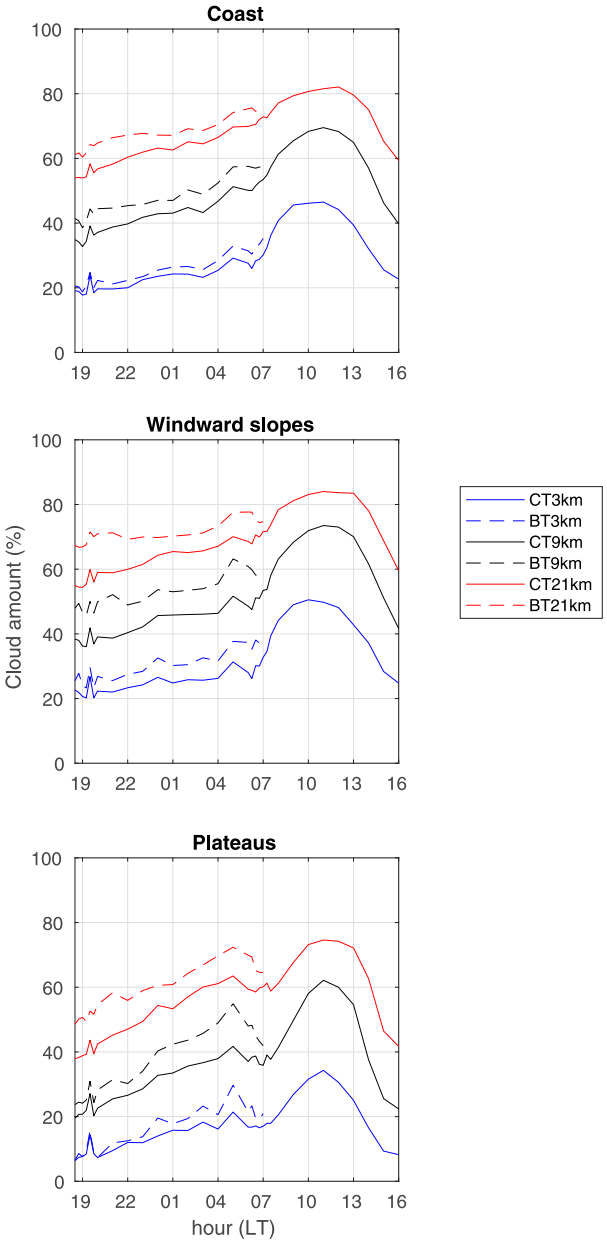

FIG. 7. ULLC amount evolution through the diurnal cycle in SAFNWC as obtained from standard (CT, full line) and specific (BT, dashed line) thresholds considering three different spatial scales—1 pixel (CT/BT 3 km), 3 × 3 (CT/BT 9 km), and 7 × 7 (CT/BT 21 km) pixels collocated with EECRA stations—for the three subregions and years 2012–14.

3) SPATIAL-SCALE ISSUES

The lack of agreement in ULLC amounts throughout the diurnal cycle between EECRA and SAFNWC in Fig. 4 could also arise from spatial-scale issues: the number of SAFNWC pixels used to document EECRA stations (3 × 3 pixels) might be too large or too small. Moreover, the new thresholds adopted appear too conservative. Therefore, the ULLC diurnal cycles in SAFNWC and for the three subregions are computed for three different boxes—that is, ~3 km × 3 km (i.e., 1 pixel), ~9 km × 9 km (3 × 3 pixels), and 21 km × 21 km (i.e., 7 × 7 pixels)—around stations. As no significant differences are observed between the cloud amounts obtained for the three boxes (results not shown), we applied a different approach for computing cloud amounts. This approach relies on the difficulty in detecting ULLC at night but also during daytime when ULLC are small cumulus (Sèze et al. 2015). ULLC amounts are not calculated by averaging the binary (cloudy vs noncloudy) pixel data for all pixels. Instead, we assume that if at least one pixel (out of 9 or 49) is cloudy, then all the pixels are cloudy, and the cloud amount is put as 100%.

Results are presented in Fig. 7. ULLC amounts remain largely underestimated (>20%) as compared to EECRA (Fig. 4b), especially during nighttime, when 1 pixel only or 3 × 3 pixels are considered. When 7 × 7 pixels are considered, for the windward slopes and plateaus, the maximal and minimal ULLC amounts become close to EECRA. However, the phase of the diurnal cycle is still shifted to the morning in SAFNWC as compared to the end of the night in EECRA. In the coastal plains, the amplitude of the diurnal cycle remains too large as compared to EECRA. We hypothesize that this is also related to the area seen by observers, probably larger than inland, so they also capture the ULLC cover over the ocean that displays a diurnal cycle of weak amplitude (Fig. 3b).

c. *Concomitant atmospheric dynamics and SSTs*

1) JJAS MEAN SEASONAL PATTERNS

The mean SSTs and atmospheric dynamics over the eastern Atlantic and WCA that co-occur with the low cloud cover are shown in Fig. 8. In JJAS, a marked meridional gradient of SSTs of ~3°C across 4° of latitude is observable along the WCA coast (Fig. 8a) with SSTs below 22°C (above 25°C) south (north) of Cape Lopez (Fig. 1). Cool SSTs off Gabon's southern coast relate to the peak of development of the Benguela upwelling to the south. JJAS is also the season of intense southerly winds off the coast (Fig. 8a). They originate from the Saint Helena high, which is at its maximal development during this season (winter in the Southern Hemisphere). Inland the winds develop a strong eastward component and penetrate as far as 18°E in response to the zonal pressure gradient that develops between the equatorial Atlantic and the Congo basin (Fig. 8a; Neupane 2016). Actually, they coincide with the subsiding and ascending

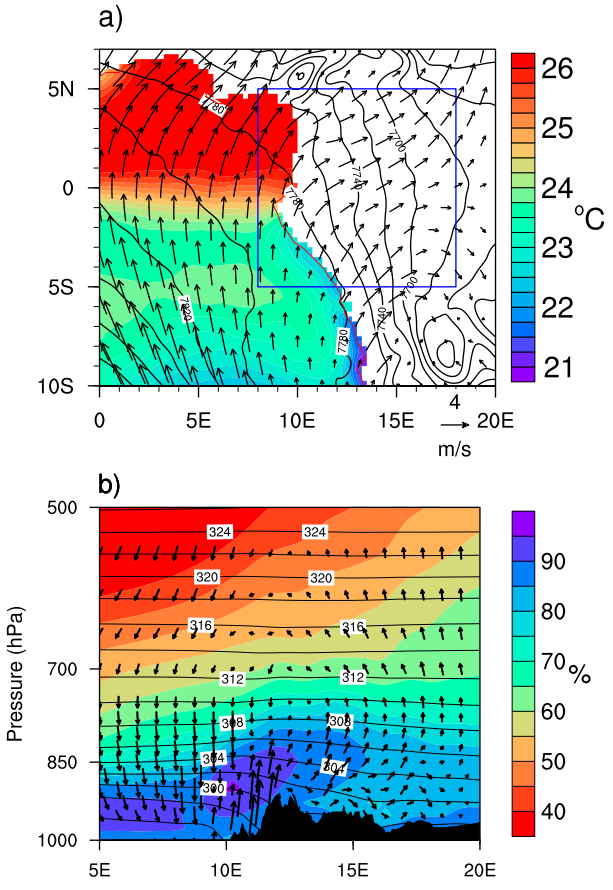

FIG. 8. (a) JJAS mean fields of SSTs (°C, OSTIA, 2009–14; shadings), wind speed and direction at 925 hPa (vectors), and geopotential ($m^2\,s^{-2}$; contours) (from ERA-STF, 2009–14). (b) JJAS longitude–altitude cross section at 2°S of the divergent component of the zonal wind ($m\,s^{-1}$), and the vertical velocity (ω, $\times 10^{-2}$ Pa s^{-1}; vectors), relative humidity (%; shadings), and equivalent potential temperature (θ, K; contours) (from ERA-STF, 2009–14).

motions observed at 8° and 18°E (Fig. 8b), respectively, alluding to the presence of a Walker overturning, zonal circulation that is well identified over central Africa and the eastern equatorial Atlantic in JJAS (Nicholson and Grist 2003; Cook and Vizy 2016; Neupane 2016). Figure 8b points also to a rapid decrease in equivalent potential temperature east of the plateaus (12°E). Moreover, JJAS is the main dry season of Gabon, with less than 1 mm day^{-1} according to TRMM rainfall (not shown). This suggests that we are in the presence of a foehn, but that type of foehn without rainfall on the windward slopes of the plateaus and warm, and adiabatically flowing air parcels coming close to the ground over and behind the plateaus. This may explain the lower frequency of ULLC there [adding to a larger influence of the Congo basin atmospheric dynamics evoked in section 3a(1)]. Besides this large-scale zonal circulation, a small-scale zonal circulation is also observed at low levels (below 600 hPa) with ascending motion by 12°E along the Mounts Cristal and Chaillu slopes (corresponding to the location of the maximum low cloud frequency in ERA-STF; Figs. 2c, S3f, and S6a) and descending motion off the coast (9°E). It indicates westerly uplift caused by topography (Mounts Cristal and Chaillu), and the resulting adiabatic exchange between coastal plains and plateaus favors the cloud formation. Indeed, when air parcels present a conditional instability, a small initial pulse is sufficient to trigger an upward movement and the formation of a cloud. But the vertical extension of such a cloud depends on the stability of the air parcels. As shown in Fig. S6c, which provides the static stability, WCA is affected by a stable air mass (values of ~1.4 K hPa^{-1}). This could explain why only low-level clouds form, which rarely evolve into higher clouds. At the surface, the wind speed (Fig. S6b) decreases rapidly as it passes over the plateaus, from about 4 m s^{-1} over the nearby Atlantic and the coastal plain to ~2.5–3.5 m s^{-1} above plateaus, the eastern slopes, and valleys. The wet air mass is also thicker over the plateaus (Fig. 8b) due to condensation associated with air uplift along the windward flanks of Mount Chaillu.

2) JJAS MEAN DIURNAL EVOLUTIONS

The evolution of the atmospheric dynamics along the diurnal cycle over WCA as provided by ERA-STF is now explored to understand the ULLC diurnal dynamics and spatial patterns. The focus is put on 1) the southern part of WCA, roughly Gabon, since Figs. 2 and 5 show that it is the area most frequently blanketed in ULLC; and 2) those days when ULLC cover is above 75% at 1300 LT for three consecutive days (area: 6°S–1°N; land-only pixels; 145 days out of 732) in SAFNWC.

Diurnal dynamics of ULLC in ERA-STF during these cloudy days is checked first. Three-hourly vertical profiles of cloud fraction averaged over 6°S–1°N and 10°–14°E are provided in Fig. 9a along with the vertical profiles of wind speed, relative humidity, and temperature (Figs. 9b–d). The cloud fraction is at its minimum (12%) at 2200 LT. During the course of the night and especially during the second part of the night, this fraction increases rapidly to reach its highest value (34%) at 0700 LT and its lowest altitude/level (~920 hPa). Between 1000 and 1300 LT, low cloud cover dissipates and ascends rapidly (~18% and ~840 hPa at 1300 LT), and then at a slower pace until 2200 LT. This is consistent with the mean diurnal cycles of EECRA low cloud amounts and base heights (cf. Fig. S7).

Low-level winds are important for cloud formation, as they control advection of moisture and temperature, and

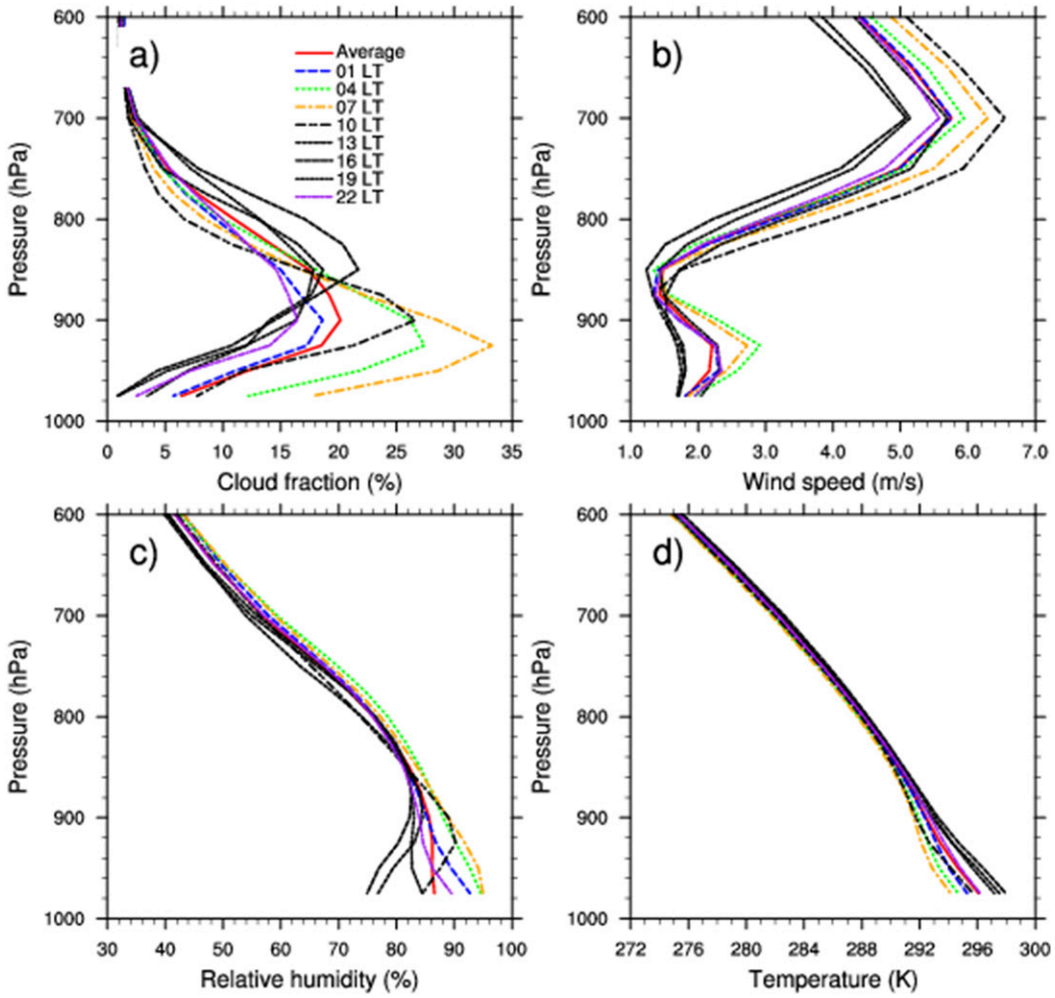

FIG. 9. ERA-STF 3-hourly vertical profiles of (a) cloud fraction (%), (b) wind speed ($m\,s^{-1}$), (c) relative humidity, and (d) temperature (K) from 1000 to 600 hPa, averaged over the longitudes 10°–14°E and latitudes 6°S–1°N for those days when the low cloud cover over Gabon at 1300 LT is above 75% for three consecutive days (2009–14, SAFNWC). The daily average is marked (red line).

contribute to turbulent mixing. The diurnal evolution of low-level wind speeds (<875 hpa; Fig. 9b) shows that they are the fastest between 0400 and 0700 LT ($3.1\,m\,s^{-1}$) and the slowest in the afternoon ($1.8\,m\,s^{-1}$ at 1500–1800 LT). However, the wind speed as pictured by ERA-STF is too low (even when grid points documenting only the coastal plains and nearby ocean are considered; not shown) to conclude in this study to the existence of a nocturnal low-level jet in WCA as observed over SWA in JAS (Schuster et al. 2013; jets usually display speeds above $6\,m\,s^{-1}$). The larger cloud fraction between 0400 and 1000 LT is associated with a greater relative humidity (by 15%) below 875 hPa (Fig. 9c), and clearly no thermal inversion (Fig. 9d). To complete the picture of the atmospheric dynamics in ERA-STF associated with cloudy days in Gabon, 3-hourly cross sections of wind, equivalent potential temperature (black lines), and relative humidity (shadings) are provided in Fig. 10. The main feature is the reversal of air motion at low levels between 0400 and 1300 LT from subsidence over WCA and the nearby Atlantic by 0700 LT to rising motion inland by noon. The 0400–0700 LT period is also characterized by large moisture content over the whole area (>85%). Ascending motion, which is observable above the coastal plain (10°E) throughout the day, is also weakest at 0400–0700 LT and is blocked by subsiding motion above 875 hPa. The 1300–1600 LT period on the other hand is characterized by ascending motion above the coastal plain and Mounts Chaillu, and a marked decrease in equivalent potential temperature. The high level of moisture, fast winds, and ascending motion below 850 hPa, which are observed between 0400 and

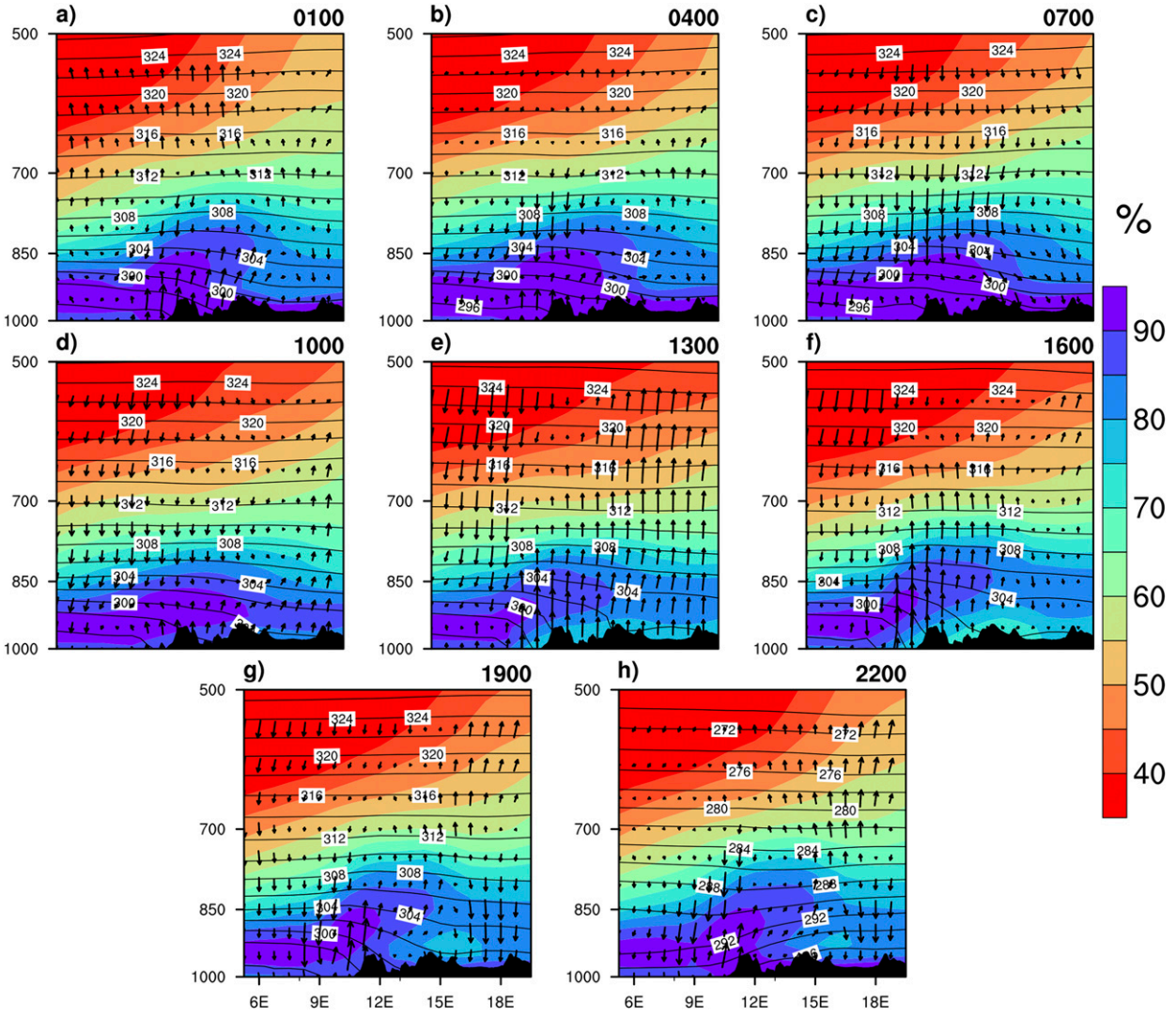

FIG. 10. ERA-STF 3-hourly (0100, 0400, 0700, 1000, 1300, 1600, 1900, 2200 LT) longitude–altitude cross sections of the divergent component of zonal wind ($m\,s^{-1}$), and the vertical velocity (ω, $\times 10^{-2}$ $Pa\,s^{-1}$; vectors), relative humidity (%; shadings), and equivalent potential temperature (θ, K; contours), at 2°S for those days when the low cloud cover over Gabon at 1300 LT is above 75% for three consecutive days (2009–14, SAFNWC).

0700 LT, could explain the development of clouds in the coastal plains and along the windward slopes of Mounts Chaillu. But they cannot evolve into higher clouds because they are overlaid with subsiding motion. Then during daytime, the surface heating (more rapid on the plateaus and eastern slopes exposed sooner to sun rays) could favor the ULLC breaking up and then rapidly dissipating earlier over the plateaus and windward slopes than over the coastal plains (afternoon).

4. Conclusions

The aim of this study was to provide a first description of the low-level cloud cover that affects western central Africa in June–September, and a first assessment of the atmospheric and nearby sea surface conditions associated with this cloud cover. Using SAFNWC, EECRA, CALIOP cloud climatologies, and ERA-STF reanalyses, our main findings in terms of ULLC mean spatial patterns, diurnal evolutions, related atmospheric dynamics, and data product limitations are the following:

- In June–September over WCA, ULLC are very common and are mainly composed of stratiform clouds, especially over Gabon and southern Congo, where frequencies from EECRA and SAFNWC are >50%. Cloud cover quickly decreases to the north and east, dropping below 25%. The rapid decrease of

ULLC to the east is partly related to a foehn effect as denoted by a decrease in equivalent potential temperature. However, comparisons with EECRA and CALIOP databases suggest that ULLC frequencies are underestimated in SAFNWC. These underestimations are not a result of masking of ULLC by high opaque clouds, as they are infrequent (e.g., <25% in CALIOP), except at the northern margins. Rather, they come from systematic failures in the nighttime detection of clouds [also noticed for SWA by Knippertz et al. (2011)] and also probably from the important load of aerosols in the atmosphere over the region in June–September, which also bias cloud detection.

- The amplitude and phase of the ULLC diurnal cycle are strongly modulated by topography. Although ULLC detection at nighttime by SAFNWC is problematic, by coanalyzing this later product with the EECRA database, it appears that amplitudes and phases evolve as follows: the coastal plains and ocean-facing valleys are the cloudiest and the diurnal cycle of ULLC there displays a low amplitude with a peak of cloudiness around 0400–0600 LT. Over the windward slopes and plateaus, the diurnal cycle of ULLC displays a higher amplitude and its phase is delayed toward 1000 LT. The downwind slopes facing the Congo basin experience less cloud cover with the daily maximum also peaking in midmorning.
- This large cloud cover is concomitant with a marked north–south SST gradient in the eastern Atlantic and cool SSTs off the Gabonese coast. A Walker overturning zonal circulation is also in place during this season over central Africa. At the diurnal scale, the cloudiest days are associated with a reversal from subsidence at 0700 LT over the coastal plains to rising motion at 1300 LT, but winds at the surface remain slow and no thermal inversion is observed. Tropospheric static stability is also in place and could explain why clouds cannot develop into higher clouds.

The products and approaches used in our study are different from those used in studies dedicated to ULLC cover over southern West Africa. For southern West Africa, studies have relied strongly on in situ measurements and case studies that enabled portraying precisely the diurnal cycle of low clouds and the dynamics associated with their setup and dissipation (Knippertz et al. 2011; van der Linden et al. 2015). The main differences between low cloud cover in SWA compared to WCA are the greater cloud frequencies in WCA than in SWA and the stronger topographic controls in WCA. The complex topography of WCA causes marked differences in the amplitude and phase of the ULLC diurnal cycle between the plains and valleys versus the plateaus and slopes. In SWA, the diurnal cycle of ULLC is uniformly phased with a peak around 1000 LT (van der Linden et al. 2015), although a foehn effect behind the Mampong range in Ghana is also clearly observed in SWA. Also in SWA, the main driver of low cloud is the presence of a nocturnal low-level jet that is not observable in WCA using ERA-STF. Nonetheless, it is noteworthy that ULLC diurnal cycles over the windward slopes and plateaus in WCA have a phase similar to ULLC in SWA: a peak around 1000 LT and a minimum around 1800 LT.

Atmospheric processes at play also appear different between SWA and WCA, even if not properly depicted in this study. The diurnal dynamics of ULLC in SWA relate to the setup and dissipation of a nocturnal low-level jet (Schuster et al. 2013), a feature that we could not reliably identify in WCA using the ERA-STF, nor a distinct thermal inversion. Inland in SWA, the forced lifting on windward slopes has been shown by the same authors to create additional cooling that contributes, along with turbulent mixing driven by the NLLJ and cool advection from the south, to ULLC formation and maintenance. Last, the season of low cloudiness is longer by ~1 month in WCA than in SWA (reported only in July–September). For western South Africa (i.e., Namibia), ULLC cover has been studied using MSG retrievals for 0800 and 1500 LT only (Cermak 2012), but over the entire annual cycle. Because of the much drier context of WSA and cooler SSTs off the coast, ULLC are clearly advected from the nearby ocean and do not spread farther than 50–100 km inland (Cermak 2012) versus 300–400 km in WCA and SWA. Their frequency is also much lower than in the two other regions (<30%).

The main limitation of this study relates to the estimation of low cloud frequency at night with large differences between EECRA and SAFNWC/CALIOP/ERA-STF. Because of the lack of updated and appropriate in situ measurements of cloudiness in WCA to compare against remote sensing estimates, we could not accurately portray the ULLC diurnal cycle, particularly in the coastal plains. The attempts made to improve the ULLC detection at night by modifying the SAFNWC thresholds do not lead to a significant improvement in ULLC detection in coastal plains. These issues could be tackled through case studies. Using data from individual days could help identify the thresholds appropriate for the region for better detection of ULLC at nighttime more easily. Individual radiosondes from the few existing stations could also provide valuable information for better understanding of the atmospheric dynamics in place. In particular, the following questions could be

resolved, Are ULLC patterns over the coastal plains driven by dynamics different from ULLC along the windward slopes and plateaus, or are the dynamics driving ULLC formation and maintenance in the windward slopes similar to those observed in SWA?

Acknowledgments. Atanas Dommo acknowledges the AUF for the funding of a 3-month stay in May–July 2016 at IGE, France. He also thanks the SCAC of the French Embassy for the funding of a one-month stay in December 2016 at IGE, France. He also acknowledges Pierre Camberlin, Pierre Couteron, Gil Mahé, and Vincent Moron, who are members of his doctoral steering committee, for their helpful comments. The authors thank the AERIS/ICARE data center (http://www.icare.univ-lille1.fr/) for providing access to the SAFNWC CT data used in this study. They also thank the three anonymous reviewers for their encouraging and constructive comments. This work was supported by the French national program INSU LEFE-IMAGO. It is also part of the International Joint Laboratory's research ''Dynamics of Land Ecosystems in Central Africa: A Context of Global Changes'' (IJL DYCOCA/LMI DYCOFAC).

REFERENCES

Bony, S., and Coauthors, 2015: Clouds, circulation and climate sensitivity. *Nat. Geosci.*, **8**, 261–268, https://doi.org/10.1038/ngeo2398.

Cermak, J., 2012: Low clouds and fog along the South-Western African coast—Satellite-based retrieval and spatial patterns. *Atmos. Res.*, **116**, 15–21, https://doi.org/10.1016/j.atmosres.2011.02.012.

Cheng, A., and K. M. Xu, 2015: Improved low-cloud simulation from the Community Atmosphere Model with an advanced third-order turbulence closure. *J. Climate*, **28**, 5737–5762, https://doi.org/10.1175/JCLI-D-14-00776.1.

Chepfer, H., G. Cesana, D. Winker, B. Getzewich, M. Vaughan, and Z. Liu, 2013: Comparison of two different cloud climatologies derived from CALIOP-attenuated backscattered measurements (level 1): The *CALIPSO*-ST and the *CALIPSO*-GOCCP. *J. Atmos. Oceanic Technol.*, **30**, 725–744, https://doi.org/10.1175/JTECH-D-12-00057.1.

Cook, K. H., and E. K. Vizy, 2016: The Congo Basin Walker circulation: Dynamics and connections to precipitation. *Climate Dyn.*, **47**, 697–717, https://doi.org/10.1007/s00382-015-2864-y.

Dee, D. P., and Coauthors, 2011: The ERA-Interim reanalysis: Configuration and performance of the data assimilation system. *Quart. J. Roy. Meteor. Soc.*, **137**, 553–597, https://doi.org/10.1002/qj.828.

Del-Val, E., J. J. Armesto, O. Barbosa, D. A. Christie, A. G. Gutiérrez, C. G. Jones, P. A. Marquet, and K. C. Weathers, 2006: Rain forest islands in the Chilean semiarid region: Fog-dependency, ecosystem persistence and tree regeneration. *Ecosystems*, **9**, 598–608, https://doi.org/10.1007/s10021-006-0065-6.

Derrien, M., and H. Le Gléau, 2005: MSG/SEVIRI cloud mask and type from SAFNWC. *Int. J. Remote Sens.*, **26**, 4707–4732, https://doi.org/10.1080/01431160500166128.

——, and ——, 2010: Improvement of cloud detection near sunrise and sunset by temporal-differencing and region-growing techniques with real-time SEVIRI. *Int. J. Remote Sens.*, **31**, 1765–1780, https://doi.org/10.1080/01431160902926632.

Donlon, C. J., M. Martin, J. D. Stark, J. Roberts-Jones, E. Fiedler, and W. Wimmer, 2012: The Operational Sea Surface Temperature and Sea Ice Analysis (OSTIA). *Remote Sens. Environ.*, **116**, 140–158, https://doi.org/10.1016/j.rse.2010.10.017.

Dufresne, J. L., and S. Bony, 2008: An assessment of the primary sources of spread of global warming estimates from coupled atmosphere–ocean models. *J. Climate*, **21**, 5135–5144, https://doi.org/10.1175/2008JCLI2239.1.

Eastman, R., and S. Warren, 2014: Diurnal cycles of cumulus, cumulonimbus, stratus, stratocumulus, and fog from surface observations over land and ocean. *J. Climate*, **27**, 2386–2404, https://doi.org/10.1175/JCLI-D-13-00352.1.

García-Santos, G., M. V. Marzol, and G. Aschan, 2004: Water dynamics in a laurel montane cloud forest in the Garajonay National Park (Canary Islands, Spain). *Hydrol. Earth Syst. Sci.*, **8**, 1065–1075, https://doi.org/10.5194/hess-8-1065-2004.

Guzman, R., and Coauthors, 2017: Direct atmosphere opacity observations from CALIPSO provide new constraints on cloud-radiation interactions. *J. Geophys. Res. Atmos.*, **122**, 1066–1085, https://doi.org/10.1002/2016JD025946.

Hannak, L., P. Knippertz, A. H. Fink, A. Kniffka, and G. Pante, 2017: Why do global climate models struggle to represent low-level clouds in the West African summer monsoon? *J. Climate*, **30**, 1665–1687, https://doi.org/10.1175/JCLI-D-16-0451.1.

Jackson, B., S. E. Nicholson, and D. Klotter, 2009: Mesoscale convective systems over western equatorial Africa and their relationship to large-scale circulation. *Mon. Wea. Rev.*, **137**, 1272–1294, https://doi.org/10.1175/2008MWR2525.1.

Jiang, J. H., and Coauthors, 2012: Evaluation of cloud and water vapor simulations in CMIP5 climate models using NASA ''A-Train'' satellite observations. *J. Geophys. Res.*, **117**, D14105, https://doi.org/10.1029/2011JD017237.

Kamsu-Tamo, P. H., S. Janicot, D. Monkam, and A. Lenouo, 2014: Convection activity over the Guinean coast and Central Africa during northern spring from synoptic to intra-seasonal timescales. *Climate Dyn.*, **43**, 3377–3401, https://doi.org/10.1007/s00382-014-2111-y.

Klein, S. A., and D. L. Hartmann, 1993: The seasonal cycle of low stratiform clouds. *J. Climate*, **6**, 1587–1606, https://doi.org/10.1175/1520-0442(1993)006<1587:TSCOLS>2.0.CO;2.

Knippertz, P., A. H. Fink, R. Schuster, J. Trentmann, J. M. Schrage, and C. Yorke, 2011: Ultra-low clouds over the southern West African monsoon region. *Geophys. Res. Lett.*, **38**, L21808, https://doi.org/10.1029/2011GL049278.

Laing, A. G., R. Carbone, and J. Tuttle, 2008: The propagation and diurnal cycles of deep convection in northern tropical Africa. *Quart. J. Roy. Meteor. Soc.*, **134**, 93–109, https://doi.org/10.1002/qj.194.

Lauer, A., and K. Hamilton, 2013: Simulating clouds with global climate models: A comparison of CMIP5 results with CMIP3 and satellite data. *J. Climate*, **26**, 3823–3845, https://doi.org/10.1175/JCLI-D-12-00451.1.

Li, J., J. Huang, K. Stamnes, T. Wang, Q. Lv, and H. Jin, 2015: A global survey of cloud overlap based on CALIPSO and CloudSat measurements. *Atmos. Chem. Phys.*, **15**, 519–536, https://doi.org/10.5194/acp-15-519-2015.

Mayaux, P., and Coauthors, 2013: State and evolution of the African rainforests between 1990 and 2010. *Philos. Trans. Roy. Soc. London*, **368B**, 20120300, https://doi.org/10.1098/rstb.2012.0300.

McGill, M. J., M. A. Vaughan, C. R. Trepte, W. D. Hart, D. L. Hlavka, D. M. Winker, and R. Kuehn, 2007: Airborne validation of spatial properties measured by the CALIPSO lidar. *J. Geophys. Res.*, **112**, D20201, https://doi.org/10.1029/2007JD008768.

Muñoz, R. C., J. Quintana, M. J. Falvey, J. A. Rutllant, and R. Garreaud, 2016: Coastal clouds at the eastern margin of the southeast Pacific: Climatology and trends. *J. Climate*, **29**, 4525–4542, https://doi.org/10.1175/JCLI-D-15-0757.1.

Neupane, N., 2016: The Congo Basin zonal overturning circulation. *Adv. Atmos. Sci.*, **33**, 767–782, https://doi.org/10.1007/s00376-015-5190-8.

Nicholson, S. E., and J. P. Grist, 2003: The seasonal evolution of the atmospheric circulation over West Africa and equatorial Africa. *J. Climate*, **16**, 1013–1030, https://doi.org/10.1175/1520-0442(2003)016<1013:TSEOTA>2.0.CO;2.

Oliveira, R. S., C. B. Eller, P. R. L. Bittencourt, and M. Mulligan, 2014: The hydroclimatic and ecophysiological basis of cloud forest distributions under current and projected climates. *Ann. Bot.*, **113**, 909–920, https://doi.org/10.1093/aob/mcu060.

Philippon, N., and Coauthors, 2016: Analysis of the diurnal cycles for a better understanding of the mean annual cycle of forests greenness in Central Africa. *Agric. For. Meteor.*, **223**, 81–94, https://doi.org/10.1016/j.agrformet.2016.04.005.

Pilié, R. J., E. J. Mack, C. W. Rogers, U. Katz, and W. C. Kocmond, 1979: The formation of marine fog and the development of fog-stratus systems along the California coast. *J. Appl. Meteor.*, **18**, 1275–1286, https://doi.org/10.1175/1520-0450(1979)018<1275:TFOMFA>2.0.CO;2.

Pokam, W. M., C. L. Bain, R. S. Chadwick, R. Graham, D. J. Sonwa, and F. M. Kamga, 2014: Identification of processes driving low-level westerlies in west equatorial Africa. *J. Climate*, **27**, 4245–4262, https://doi.org/10.1175/JCLI-D-13-00490.1.

Roberts, G., M. J. Wooster, and E. Lagoudakis, 2009: Annual and diurnal African biomass burning temporal dynamics. *Biogeosciences*, **6**, 849–866, https://doi.org/10.5194/bg-6-849-2009.

Sassen, K., Z. Wang, and D. Liu, 2009: Cirrus clouds and deep convection in the tropics: Insights from CALIPSO and CloudSat. *J. Geophys. Res.*, **114**, D00H06, https://doi.org/10.1029/2009JD011916.

Schrage, J. M., and A. H. Fink, 2012: Nocturnal continental low-level stratus over tropical West Africa: Observations and possible mechanisms controlling its onset. *Mon. Wea. Rev.*, **140**, 1794–1809, https://doi.org/10.1175/MWR-D-11-00172.1.

——, S. Augustyn, and A. H. Fink, 2007: Nocturnal stratiform cloudiness during the West African monsoon. *Meteor. Atmos. Phys.*, **95**, 73–86, https://doi.org/10.1007/s00703-006-0194-7.

Schuster, R., A. H. Fink, and P. Knippertz, 2013: Formation and maintenance of nocturnal low-level stratus over the southern West African monsoon region during AMMA 2006. *J. Atmos. Sci.*, **70**, 2337–2355, https://doi.org/10.1175/JAS-D-12-0241.1.

Sèze, G., J. Pelon, M. Derrien, H. Le Gléau, and B. Six, 2015: Evaluation against CALIPSO lidar observations of the multi-geostationary cloud cover and type dataset assembled in the framework of the Megha-Tropiques mission. *Quart. J. Roy. Meteor. Soc.*, **141**, 774–797, https://doi.org/10.1002/qj.2392.

Subrahmanyam, K. V., and K. K. Kumar, 2016: CloudSat observations of multi layered clouds across the globe. *Climate Dyn.*, **49**, 327–341, https://doi.org/10.1007/s00382-016-3345-7

Torregrosa, A., C. Combs, and J. Peters, 2016: GOES-derived fog and low cloud indices for coastal north and central ecological analyses. *Earth Space Sci.*, **3**, 46–67, https://doi.org/10.1002/2015EA000119.

Torres, O., P. K. Bharta, J. R. Herman, A. Sinyuk, P. Ginoux, and B. Holben, 2002: A long-term record of aerosols optical depth from TOMS observations and comparison to AERONET measurements. *J. Atmos. Sci.*, **59**, 398–413, https://doi.org/10.1175/1520-0469(2002)059<0398:ALTROA>2.0.CO;2.

van der Linden, R., A. H. Fink, and R. Redl, 2015: Satellite-based climatology of low-level continental clouds in southern West Africa during the summer monsoon season. *J. Geophys. Res. Atmos.*, **120**, 1186–1201, https://doi.org/10.1002/2014JD022614.

Vondou, D. A., A. Nzeukou, A. Lenouo, and F. Mkankam Kamga, 2010: Seasonal variations in the diurnal patterns of convection in Cameroon–Nigeria and their neighboring areas. *Atmos. Sci. Lett.*, **11**, 290–300, https://doi.org/10.1002/asl.297.

Wilson, A. M., and W. Jetz, 2016: Remotely sensed high-resolution global cloud dynamics for predicting ecosystem and biodiversity distributions. *PLoS Biol.*, **14**, e1002415, https://doi.org/10.1371/journal.pbio.1002415.

Winker, D. M., M. Vaughan, A. Omar, Y. Hu, and K. A. Powell, 2009: Overview of the CALIPSO mission and CALIOP data processing algorithms. *J. Atmos. Oceanic Technol.*, **26**, 2310–2323, https://doi.org/10.1175/2009JTECHA1281.1.